J Mater Sci (2012) 47:341–349
DOI 10.1007/s10853-011-5803-2

Preparation of porous spherical ZrO_2–SiO_2 composite particles using templating and its solid acidity by H_2SO_4 treatment

Shuhei Uchiyama · Toshihiro Isobe · Sachiko Matsushita · Kiyotaka Nakajima · Michikazu Hara · Akira Nakajima

Received: 24 May 2011 / Accepted: 18 July 2011 / Published online: 27 July 2011

Abstract Porous ZrO_2–SiO_2 composite sphere particles were prepared by impregnating precursor solutions into organic monolith particles, with subsequent calcination in air. The porous spheres possessed uniformly sized pores of around 10 nm. Addition of SiO_2–ZrO_2 decreased the ZrO_2 crystallinity and increased the specific surface area. The acid amount on the surface of the composite spheres was increased by treatment with H_2SO_4. The acid strength and its amount, including the Lewis/Brønsted acid ratio, depended on the SiO_2/ZrO_2 ratio and the H_2SO_4 concentration. The powder treated under an optimum condition exhibited higher solid acidity than the reference solid acid catalyst. The prepared porous SO_4^{2-}/ZrO_2–SiO_2 spheres showed higher saccharization activity than the reference solid acid catalyst did.

Introduction

Controlling the pore structure of porous materials during synthesis is of great importance because these structural characteristics strongly influence the performance of the materials. Templating is a promising method for fabrication of inorganic materials with controlled morphology and inner structural arrangements. The fabrication process involves the infiltration of precursor solutions into the interstice of templates and subsequent removal of the templates by calcination or extraction [1, 2]. Mesoporous silica and related materials are the most well-known materials obtained from the templating process [3–10]. However, precise process control is necessary for the processing of these materials. Moreover, the pore walls are extremely thin and are too weak for handling. Consequently, practical application fields for these materials are few.

In contrast, solid acid catalysts have a surface with acid points. They function as an acid under a solid state. These materials have attracted much attention from the viewpoint of green chemistry because of the feasibility of their repeated use and easy separation of products. In general, they are characterized by their Brønsted and/or Lewis acidity, the strength and number of sites, and surface area and porosity. Although zeolites are widely used as solid acid catalysts, their small (<1 nm) pores make them unsuitable for the decomposition of large molecules such as biomass substances [11].

Great interest has surrounded the use of sulfated metal oxides as strong solid acids, in particular sulfated zirconia, which might possess superacidic properties [12–22]. This material is prepared conventionally by treating amorphous ZrO_2 with H_2SO_4 solutions and subsequent calcinations around 500 °C. During calcination, complicated processes such as dehydration, crystallization (into tetragonal (major) and monoclinic (minor) phases), and bonding of sulfate species onto ZrO_2 surface take place in materials. The typical specific surface area of the catalyst is 80–100 m^2/g

Electronic supplementary material The online version of this article (doi:10.1007/s10853-011-5803-2) contains supplementary material, which is available to authorized users.

S. Uchiyama · T. Isobe · S. Matsushita · A. Nakajima (✉)
Department of Metallurgy and Ceramic Science, Graduate School of Science and Engineering, Tokyo Institute of Technology, 2-12-1 O-okayama, Meguro-ku, Tokyo 152-8552, Japan
e-mail: anakajim@ceram.titech.ac.jp

K. Nakajima · M. Hara
Materials and Structures Laboratory, Tokyo Institute of Technology, 4259 Nagatsuta-cho, Midori-ku, Yokohama 226-8503, Japan

[23], with pore sizes of 3–4 nm [11]. Although greater specific surface area can be achieved using a mesoporous structure or mixing with SiO_2 [23–30], very few investigations have simultaneously examined the preparation of sulfated ZrO_2 with a large specific surface area and narrow mesopore size distribution [31].

In addition to a large specific surface area and narrow mesopore size distribution, the spherical particle morphology is suitable because it allows for good transport properties through the packed beads. As of now, several investigations have been conducted of the processing of inorganic porous spheres using template method [32–35]. However, these investigations mainly examine material processing: examinations of material performance remain insufficient.

Based on this background, we used a simple processing method to prepare spherical ZrO_2-based solid acid particles with a large specific surface area, narrow mesopore size distribution, and a certain handling strength by templating processes. Sulfate acid treatment was conducted to increase solid acidity. A silicon source was added to a precursor solution of ZrO_2 to increase the specific surface area. Then we investigated the effects of the chemical composition on the acid amount.

Experimental

Sample preparation

At the beginning of this investigation, we performed preliminary experiments for sample preparation by changing starting materials and their concentrations. Results revealed that organic monolith powder of polymethylmethacrylate is suitable for this process because of its decomposition behavior during calcination. Moreover, Zr-alkoxides such as zirconium butoxide are unsuitable as a starting zirconium source because of carbonization and resultant grayish coloration after calcination around 600 °C. We therefore determined the following experimental conditions for sample preparation.

Reagent-grade zirconium oxychloride ($ZrOCl_2{\cdot}8H_2O$; Wako Pure Chemical Industries, Ltd., Tokyo Japan, 4.8 g) was dissolved into methanol (15 mL) with tetraethyl orthosilicate (TEOS; Wako Pure Chemical Industries, Ltd.). The fractions of TEOS against the methanol solution of $ZrOCl_2{\cdot}8H_2O$ were varied from 0–20 vol%.

The solution was mixed and impregnated into organic monolith particles (MBP-8, 2.0 g; Sekisui Plastics Co., Ltd., Osaka, Japan) at room temperature. Then the suspension was stirred for 1 day. A wet monolithic powder was obtained through centrifuging at 2000 rpm for 20 min. The obtained powder was dried at 90 °C with vibration to avoid contact between the powders and was subsequently calcined at 600 °C for 1 h. The obtained samples were designated as xSi, where x corresponds to the volume fraction of TEOS in the initial methanol solution. Therefore, 20Si represents 20 vol% TEOS in the initial ZrO_2 precursor solution.

The obtained powder (0.5 g) was dispersed into various concentrations (0.0025–2.5 M) of sulfuric acid solution (5 mL). After ultrasonication (5 min) and vacuum impregnation (30 min), the powder was washed using distilled water and dried at 60 °C for 1 day. Heat treatment was then conducted at 500 °C for 1 h in ambient air.

Evaluation

Using X-ray diffraction (XRD-6100; Shimadzu Corp., Tokyo, Japan), we evaluated the powder crystalline phase. The powder morphology was observed using a field-emission scanning electron microscope (S-4500; Hitachi, Ltd., Tokyo, Japan). The specific surface area and pore size distribution were evaluated using BET method with N_2 (Autosorb-1; Quantachrome Instruments, Boynton Beach, FL, USA). The concentrations of Zr, Si, and S on the powder surface were measured using X-ray photoelectron spectroscopy (XPS, PHI Quantera SXM; PHI Co., U.S.A.) with an Al Kα X-ray line (1486.6 eV). The binding energy scales were referenced to 284.5 eV, as determined by locations of peaks on the C1 s spectra of hydrocarbon (CH_x) for correcting the deviation.

The acid quality was evaluated using pyridine adsorption. The sample powder (50 mg) was heated at 350 °C under vacuum in a special cell for 3 h. After gradual pyridine adsorption to this sample at room temperature, heating was conducted at 120 °C under vacuum for 1 h to remove physisorbed molecules. Then the infrared spectra of the powder were recorded using a Fourier transform infrared spectrophotometer (FT–IR, 8600PC; Shimadzu Corp., Kyoto, Japan).

The surface acid concentration was evaluated using temperature-programmed desorption (TPD) with NH_3 (Multitasc TPD; BEL Japan, Inc., Osaka, Japan). After pretreatment to remove adsorbed water, NH_3 adsorption was performed at 100 °C. Then the temperature was increased at the rate of 10 K/min. The amount of desorbed NH_3 during this process was evaluated. In this evaluation, the K10 acid (a montmorillonite-based solid-acid catalyst [36, 37]; Sigma-Aldrich Co., U.S.A.) amount was set as 85 μmol/g.

Practical decomposition activity by the prepared acid was evaluated using cellulose, as described in an earlier report [38]. Cellulose (0.025 g; Merck & Co., Inc., USA), the obtained powder sample (0.3 g), and water (1.0 mL) were mixed and reacted at 100 °C for 3 h. Then after

2.0 mL of water was added to the mixture, the liquid was separated from the solid by centrifugation at 4000 rpm for 2 min. The liquid composition was analyzed using high-performance liquid chromatography (HPLC, C-2000 Plus; Nihon-bunko Co., Tokyo Japan) with an RI detector and an Aminex HPX-87H column (Bio-Rad Laboratories Inc., Hercules, CA, USA).

Results and discussion

Characterization of powder composites

Figure 1 portrays SEM micrographs of starting organic monolith particles and the obtained ZrO_2–SiO_2 composite (20Si) porous spheres. The organic monolith particles were porous. Interconnected mesopores were observed on the surface (Fig. 1a, b). Comparison of the organic monolith particles with prepared ZrO_2–SiO_2 composite particles revealed inherent structural similarities: both types were spherical and porous (Fig. 1c). A cross-section image of a ZrO_2–SiO_2 composite particle obtained using a focused ion beam (Fig. 1d) revealed that the inside is also porous and that the pores are mutually interconnected. Spherical porous ZrO_2–SiO_2 composite particles were prepared using organic monolith particles. Figure 2 shows X-ray diffraction patterns of ZrO_2–SiO_2 composite particles. When TEOS was not added, the monoclinic and tetragonal ZrO_2 were crystallized. These crystalline phases gradually disappeared with increased addition of TEOS, suggesting that SiO_2 suppresses ZrO_2 crystallization. This result corresponds to those described in previous reports [26, 39].

Figure 3 presents the TEOS concentration dependence of specific surface area for the obtained ZrO_2–SiO_2 composite particles. The specific surface area increased concomitantly with increasing TEOS concentration, reaching around 190 m^2/g. Additional experiments revealed that the increase of the TEOS amount greater than 20 vol% provides larger specific surface area, but that H_2SO_4 treatment decreased the entire acid amount because the sulfate ion preferably coordinates to Zr site and provides an acid site [25]. Therefore, in this study, the maximum TEOS concentration was set as 20 vol%. Figure 4 presents the TEOS concentration dependence of pore size distribution for obtained ZrO_2–SiO_2 composite particles. The ratio of mesopores increased gradually. For the case of 20Si, its distribution was sharp and its mode value was around 10 nm. The obtained pore volumes were, respectively, 0.21, 0.25, 0.26, and 0.38 (mL/g) for 0Si, 5Si, 10Si, and 20Si. Addition of TEOS to ZrO_2 precursor solution increases the specific surface area effectively and provides mesopores with a sharp size distribution, probably because

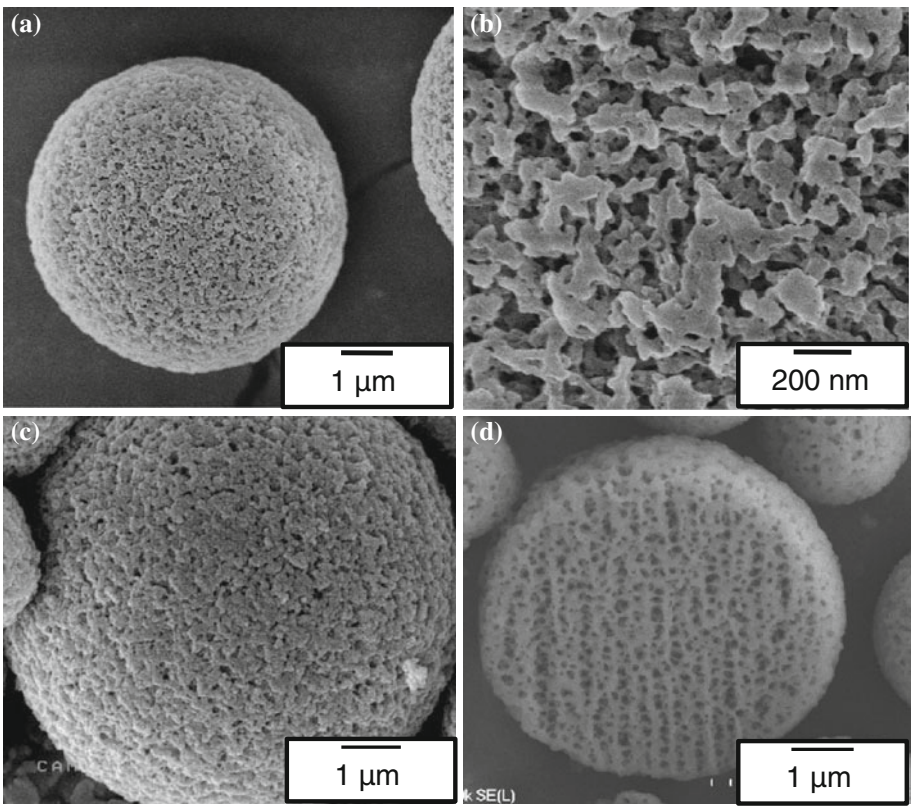

Fig. 1 SEM micrographs of starting organic monolith particles (**a**, **b**) and obtained ZrO_2–SiO_2 composite (20Si) porous spheres (**c**, **d**), where **d** is a cross section by focused ion beam.)

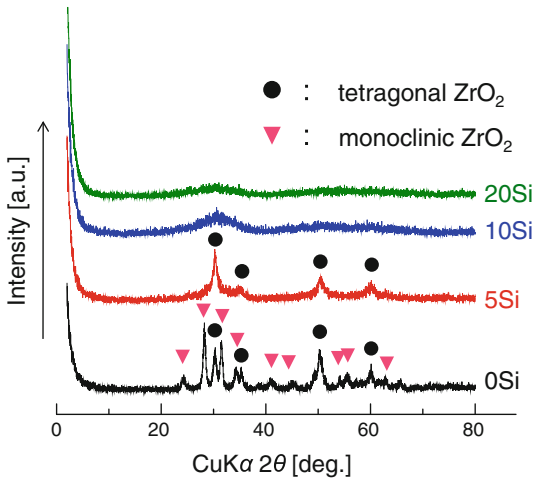

Fig. 2 X-ray diffraction patterns of ZrO_2–SiO_2 composite particles

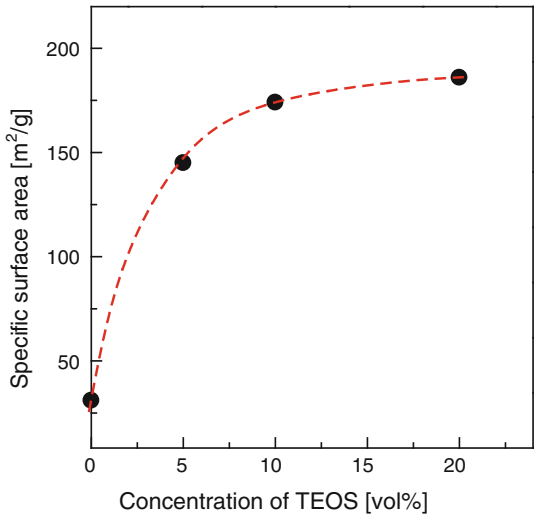

Fig. 3 TEOS concentration dependence of specific surface area for obtained ZrO_2–SiO_2 composite particles

of the suppression of ZrO_2 crystallization and the resultant inhibition of sintering. Subsequently, H_2SO_4 treatment was conducted mainly on 20Si powder because of its large specific surface area and sharp pore size distribution of the meso-order range.

Acidity and catalytic activity

Figure 5 depicts TPD spectra of 20Si powders with H_2SO_4 treatment under various concentrations. The corresponding acid amounts are presented in Table 1. XRD measurements revealed that all samples from 20Si were in an amorphous state after H_2SO_4 treatment. Both the acid amount (peak area) and acid strength (peak tailing to higher temperature) increased along with increasing acid concentration up to 1.0 M. The figure also presents the TPD spectra of the

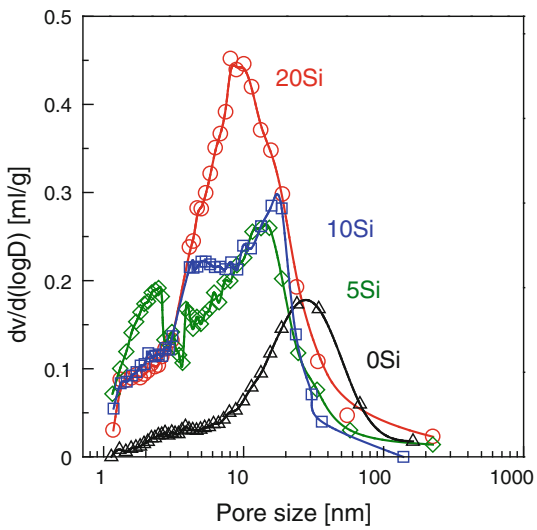

Fig. 4 TEOS concentration dependence of pore size distribution for obtained ZrO_2–SiO_2 composite particles

reference sample (Lot No. JRC-SZ-1, a standard sample of sulfated ZrO_2 provided by the Catalyst Society of Japan, specific surface area measured using N_2 adsorption was 71 m^2/g. The XRD pattern and SEM micrograph of this reference material are presented in Supporting Information.) When 20Si powder was treated with 1.0 M H_2SO_4, the total acid amount of the sample exceeded that of the reference sample, although the total acid amount decreased when the powder was treated with 2.5 M H_2SO_4. The acid amount of 20Si treated with 1.0 M H_2SO_4 did not decrease even after washing in water (100 mg powder in 100 mL water for 1 h), indicating that almost all sulfate groups are bonded directly to ZrO_2, and that the concentration of physically adsorbed (water-soluble) sulfate is extremely low. It is noteworthy that higher concentrations of acid were found on the powder treated with 2.5 M H_2SO_4 than that treated with 1.0 M H_2SO_4 despite a lower overall acid amount.

Figures 6, 7, 8 show the H_2SO_4 concentration-dependence of specific surface area, the Zr/Si ratio, and surface S concentration. Figures 7 and 8 were obtained from XPS analyses. The signal of Cl was not identified in this measurement. Both the specific surface area and the Zr/Si ratio decreased when the powder was treated using 2.5 M H_2SO_4, although the surface S concentration increased concomitantly with increasing H_2SO_4 concentration. Figures 9 and 10, respectively, depict XPS spectra of Zr3d, Si2p, S2p, and O1 s peaks. Zirconium 3d spectra showed a doublet signal at around 182.6 and 184.9 eV. These values are consistent with Zr(IV) sites in ZrO_2 [29]. Moreover, the overall peak intensity was remarkably lower for the powder treated by 2.5 M H_2SO_4. The mode value of the Si2p peak was 102.4 eV before H_2SO_4 treatment, but it shifted to

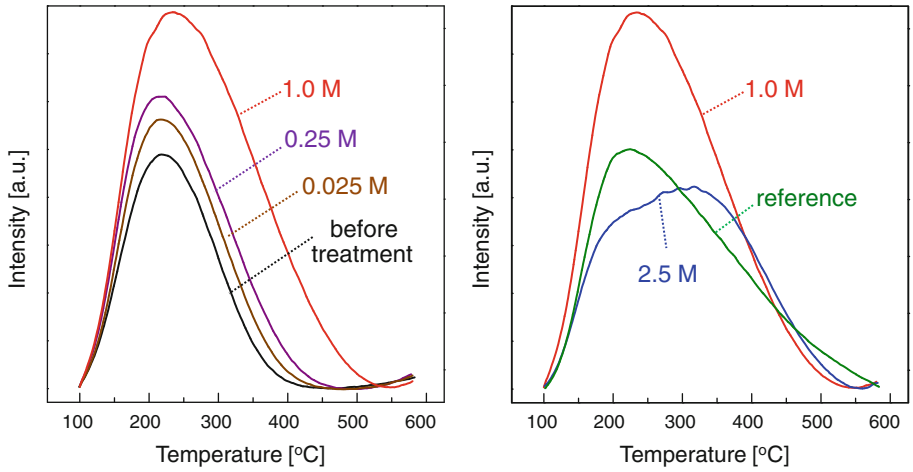

Fig. 5 TPD spectra of 20Si powders with H_2SO_4 treatment under various concentrations

Table 1 Acid amounts of 20Si powders with H_2SO_4 treatment under various concentrations

	Total acid amount (μmol/g)
Before treatment	131
0.0025 M	142
0.025 M	159
0.25 M	185
1.0 M	293
2.5 M	194
Reference	203

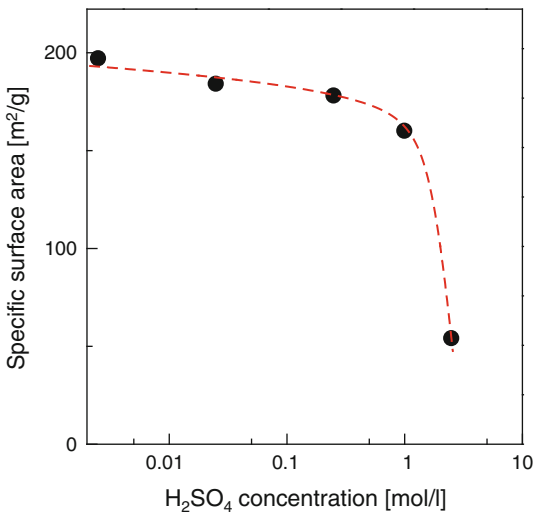

Fig. 6 H_2SO_4 concentration dependence of the specific surface area

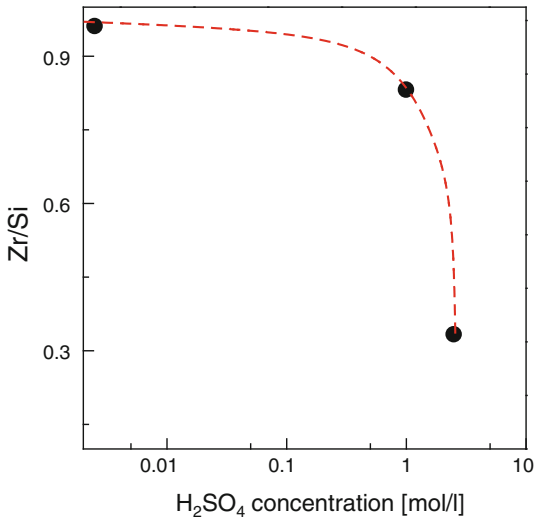

Fig. 7 H_2SO_4 concentration dependence of the Zr/Si ratio on the powder surface

102.8 eV after H_2SO_4 treatment, which suggests preferable coordination of the sulfate ion to Zr site and the resultant increase of Si–O bonding. Similar binding energy values have been described in earlier reports [29]. The overall peak intensity of Si2p is remarkably higher for the powder treated with 2.5 M H_2SO_4. This trend is opposite that of Zr3d. The intensity of S2p increased along with the increasing concentration of H_2SO_4 used for the treatment. The mode value of binding energy was around 169.3 eV. Ecormier et al. [11] attributed the decrease of the Zr signal and the increase of S signal to the formation of a chemisorbed sulfoxy overlayer. However, decreased specific surface area, overall acid amount, and Lewis acid (as described in the FT–IR section) also present the possibility of dissolution of amorphous ZrO_2 by the attack of acid [28] and the resultant change in pore structure. Probably, both phenomena occur simultaneously. For the O1 s peak, the peak separation provides three distinct peaks around 533.6, 532.2, and 530.2–530.7 eV. The first peak is attributable to water or OH groups. The second is attributed to Si–O, S–O*x*, or other hydrocarbons [40–43]. The last one originated from Zr–O [29]. The intensity of the first peak is slight and constant. The second peak intensity increases

and the third peak intensity decreases concomitantly with increasing H_2SO_4 concentration. These trends correspond to the increase of S concentration. It is noteworthy that the binding energy of the value of the third peak decreases gradually, concomitantly with the increasing H_2SO_4 concentration (530.7, 530.5, 530.5, and 530.2 eV for before treatment, 0.025, 1.0, 2.5 M, respectively.), suggesting the direct coordination of Zr atoms to electron-withdrawing SO*x* centers.

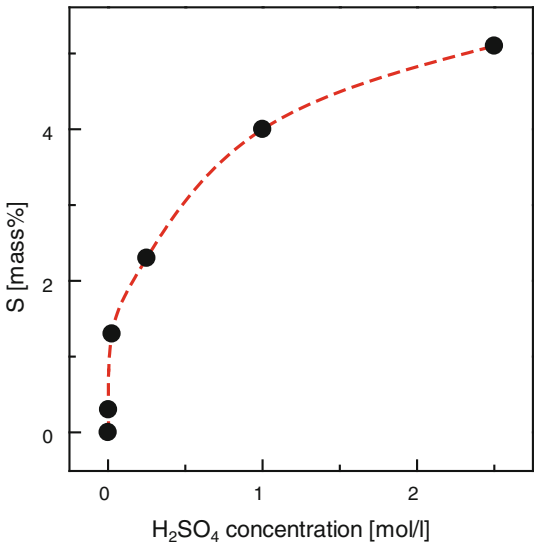

Fig. 8 H_2SO_4 concentration dependence of S concentration on the powder surface

Figure 11 presents results of FT–IR spectra for pyridine adsorption. Comparison between 0Si and 20Si revealed that the peaks for Brønsted acid around 1550 cm^{-1} and Lewis acid around 1440 cm^{-1} increased merely by adding SiO_2–ZrO_2. A schematic illustration of both acid points is presented in Fig. 12a. Many reports in the literature [44–46] describe that new surface acidic sites of mixed oxides are formed because of the difference of electronegativity between the two cations. Other reports describe that the number of the solid acid sites is expected to be proportional to the number of Zr–O–Si bands [39, 47]. When H_2SO_4 treatment was performed in this study, the number of Brønsted acid points increased along with the increasing H_2SO_4 concentration. The formation of an additional Brønsted acid point will be given to the surface by coordinating the sulfuric group on the Zr site, as shown in Fig. 12b.

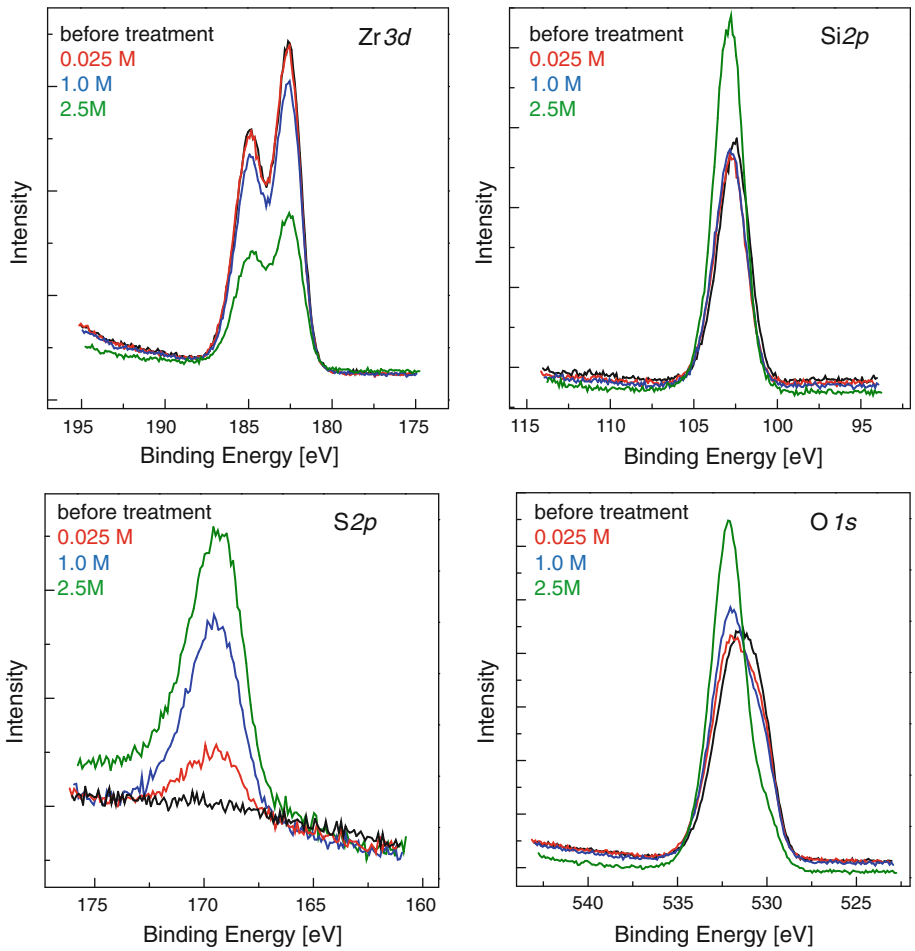

Fig. 9 XPS spectra of Zr3d, Si2p, S2p, and O1s peaks

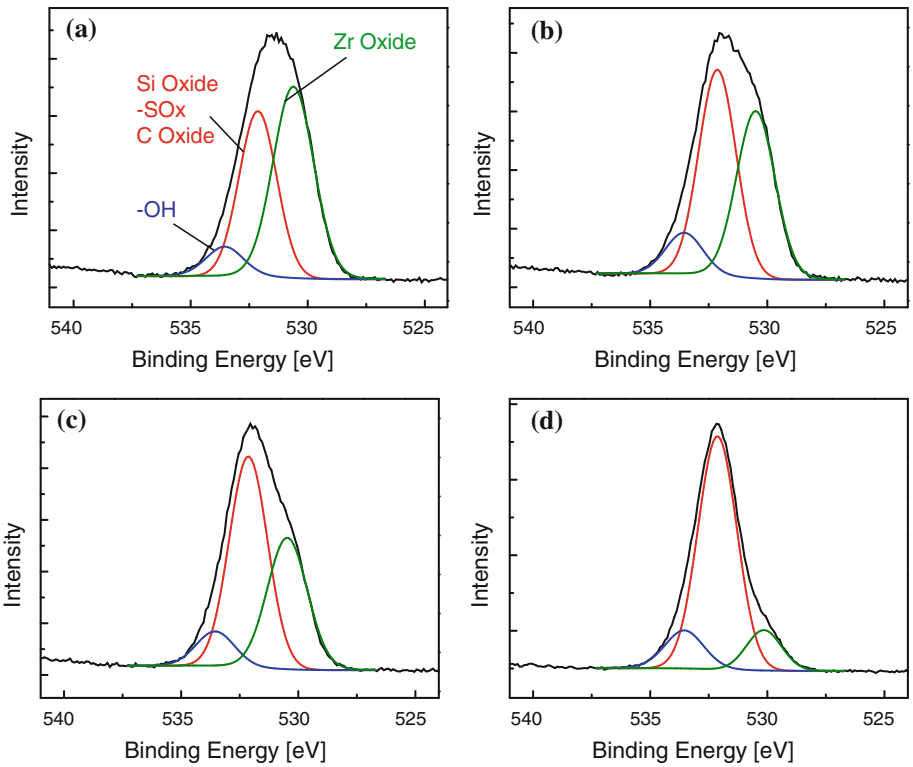

Fig. 10 Results of peak separation for O*1 s* peak by XPS analysis: **a** before treatment, **b** 0.025 M H_2SO_4, **c** 1.0 M H_2SO_4, and **d** 2.5 M H_2SO_4

The addition of SiO_2 increased the overall acid amount by increasing the surface area and by providing acid points with medium strength. However, excess addition decreased the ZrO_2 concentration where the sulfate ion preferably coordinates, and decreased the overall entire acid amount. A similar relation was also observed for the H_2SO_4 concentration dependence for 20Si powder. The thin (less than 1.0 M) H_2SO_4 treatment increased both the acid amount and its strength because of sulfate ion coordination to Zr site. However, when the H_2SO_4 concentration was 2.5 M, the overall acid amount decreased, probably because of Zr dissolution and the resultant small specific surface area.

For this study, we used the 1.0 M H_2SO_4 treatment sample to evaluate decomposition activity using cellulose. Cellulose is more abundant than starch for use as the starting material of bio-ethanol [48, 49], but decomposition of cellulose is more difficult than that of starch. Industrial producers commonly carry out this reaction using H_2SO_4. Figure 13 presents an HPLC chart of cellulose decomposition using the 3 h reaction sample. The strong peak in the figure represents that for solvent. The peak of glucose, which appeared around 11 min, with a corresponding amount of 2.1 μmol, was observed when sulfated 20Si powder was used. Additional experiments revealed that this reaction depends on the water amount, and that 6.8 μmol of glucose was obtained when the water amount was tripled. When reference sulfated ZrO_2 powder was used instead of this powder at the same practical mass ratio, glucose was not detected. This difference of glucose contents is probably attributable to differences of pore structures and acid amounts.

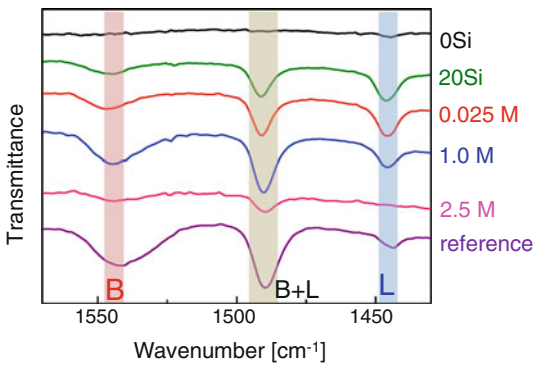

Fig. 11 FT–IR spectra for pyridine adsorption

Figure 14 portrays the pore size distribution of these two samples. The particle size of cellulose used in this study is 20–100 μm [38]. For 20Si, cellulose is decomposed initially into polysaccharides on the surface. Polysaccharides are then decomposed in turn into smaller saccharides. Once they become smaller than the pore size, the inner pore also becomes a reaction field and contributes to glucose production. Nevertheless, the decomposition reaction mainly advances on the powder surface because the pore size of the reference catalyst is small. In addition, the glucose production rate is lower than that of sulfated 20Si powder. No remarkable fracture was observed in the obtained

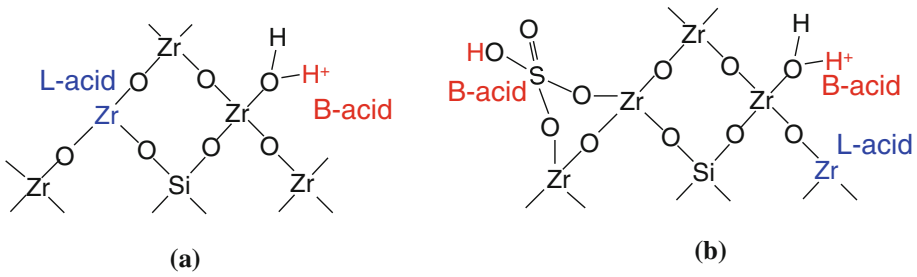

Fig. 12 Schematic illustration of expected acid points **a** before and **b** after H_2SO_4 treatment

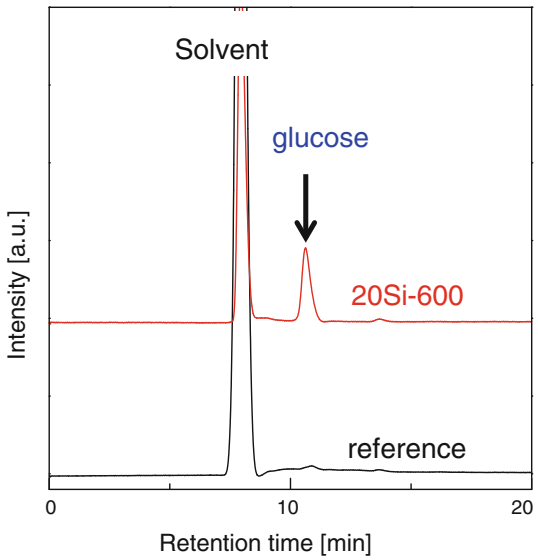

Fig. 13 HPLC chart of the cellulose decomposition using the 3 h reaction sample

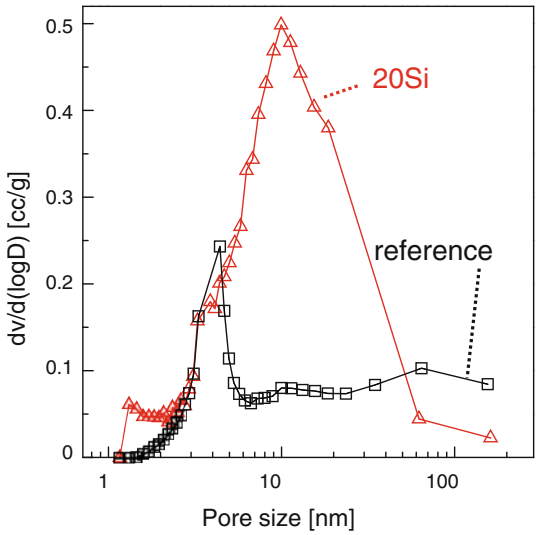

Fig. 14 Pore size distribution of the reference sample and 20Si powder after 1.0 M H_2SO_4 treatment

porous ZrO_2-based solid acid spheres through all evaluation procedures even without special care, suggesting that the particles can be handled to a certain degree.

Results of this study demonstrate that the processing of porous spherical sulfated ZrO_2–SiO_2 composite particles is feasible using organic monolith particles as a template. The powder performance is expected to depend on the processing conditions. Particularly, the homogeneity of the SiO_2–ZrO_2 is a key factor. A remarkable decrease of the specific surface area under high H_2SO_4 concentration may suggest that some segregation exists between these two components in the structure. Optimization of the process conditions, which might yield better performance, will be addressed in future work.

Conclusion

For this study, we prepared porous ZrO_2–SiO_2 composite sphere particles impregnating precursor solutions into organic monolith particles and subsequent calcination in air. The obtained porous spheres possessed a sharp pore size distribution in the mesopore range. Crystallization of ZrO_2 was suppressed, and the specific surface area was increased by the addition of SiO_2. The acid amount on the composite spheres is increased by treatment with H_2SO_4 up to 1.0 M. Acid strength and its amount; including the Lewis/Brønsted acid ratio, depend on the process conditions and chemical composition. The powder treated under optimum conditions exhibited higher solid acidity than the reference solid acid catalyst. The prepared porous sulfated ZrO_2–SiO_2 spheres exhibited better saccharization activity than the reference solid acid catalyst.

Acknowledgements The authors are grateful to staff of the Center of Advanced Materials Analysis at Tokyo Institute of Technology for SEM observations.

References

1. Deshpande AS, Niederberger M (2007) Micropor Mesopor Mater 101:413
2. Naydenov V, Tosheva L, Sterte J (2003) Micropor Mesopor Mater 66:321
3. Valde′s-Soli′s T, Fuertes AB (2006) Mater Res Bull 41:2187
4. Schuth F (2001) Chem Mater 13:3184

5. Ryoo R, Joo SH, Jun S (1999) J Phys Chem B 103:7743
6. Jun S, Joo SH, Ryoo R, Kruk M, Jaroniec M, Liu Z, Ohsuna T, Terasaki O (2000) J Am Chem Soc 122:10712
7. Zhu K, Yue B, Zhou W, He H (2003) Chem Commun 98
8. Yao BD, Zhang LD (1999) J Mater Sci 34:5983. doi: 10.1023/A:1004780728297
9. Orlov A, Zhai QZ, Klinowski J (2006) J Mater Sci 41:2187. doi: 10.1007/s10853-006-7184-5
10. Ma TY, Zhang XJ, Yuan ZY (2009) J Mater Sci 44:6775. doi: 10.1007/s10853-009-3576-7
11. Ecormier MA, Wilson K, Lee AF (2003) J Catal 215:57
12. Arata K, Hino M (1990) Mater Chem Phys 26:213
13. Arata K (1996) Appl Catal A 146:3
14. Song X, Sayari A (1996) Catal Rev 38:329
15. Xia Q-H, Hidajat H, Kawi S (2002) J Catal 205:318
16. Yadav GD, Nair JJ (1999) Micropor Mesopor Mater 33:1
17. McIntosh DJ, Kydd RA (2000) Micropor Mesopor Mater 37:281
18. Armendariz H, Coq B, Tichit D, Dutartre R, Figueras F (1998) J Catal 173:345
19. Parvulescu V, Coman S, Grange P, Parvulescu VI (1999) Appl Catal A Gen 176:27
20. Hino M, Arata K (1980) J Chem Soc Chem Commun 851–852
21. Hino M, Arata K (1979) J Am Chem Soc 101:6439
22. Wang Y, Ma JH, Liang D, Zhou MM, Li FX, Li RF (2009) J Mater Sci 44:6736. doi:10.1007/s10853-009-3603-8
23. Yang X, Jentoft FC, Jentoft RE, Girgsdies G, Ressler T (2002) Catal Lett 81:25
24. Ecormier MA, Lee AF, Wilson K (2005) Micropor Mesopor Mater 80:301
25. Sohn JR, Jang HJ (1991) J Mol Catal A 64:349
26. Miller JB, Ko EI (1996) Chem Eng J 64:273
27. Navio JA, Colon G, Macias M, Campelo JM, Romero AA, Marinas JM (1996) J Catal 161:605
28. Lopez T, Navarrete J, Gomez R, Novaro O, Figueras F, Armendariz H (1995) Appl Catal A 125:217
29. Rosenberg DJ, Coloma F, Anderson JA (2002) J Catal 210:218
30. Rosenberg DJ, Bachiller-Baeza B, Dines TJ, Anderson JA (2003) J Phys Chem B 107:6526
31. Das SK, Bhunia MK, Sinha AK, Bhaumik A (2009) J Phys Chem C 113:8918
32. Shchukin DG, Caruso RA (2004) Chem Mater 16:2287
33. Du K-F, Yang D, Sun Y (2009) Ind Eng Chem Res 48:755
34. Smatt J-H, Schuwer N, Jarn M, Lindner W, Linden M (2008) Micropor Mesopor Mater 112:308
35. Shimura N, Ogawa M (2007) J Mater Sci 42:5299. doi: 10.1007/s10853-007-1771-y
36. Soriente A, Arienzo R, Rosa MD, Spinella A, Scettri A, Palombi L (1999) Green Chem 1:157
37. Dhakshinamoorthy A, Pitchumani K (2008) Tetrahedron Lett 49:1818
38. Suganuma S, Nakajima K, Kitano M, Yamaguchi D, Kato H, Hayashi S, Hara M (2008) J Am Chem Soc 130:12787
39. Zhang Y, Pan L, Gao C, Wang Y, Zhao Y (2010) J Sol–Gel Sci Technol 56:27
40. Pouilleau J, Devilliers D, Groult H, Marcus P (1997) J Mater Sci 32:5645. doi:10.1023/A:1018645112465
41. Stoch J, Lercher J, Ceckiewicz S (1992) Zeolite 12:81
42. Zhu X, Meng Z (1994) J Appl Phys 75:3756
43. Zhang G, Sun S, Yang D, Dodelet J-P, Sacher E (2008) Carbon 46:196
44. Zhuang Q, Miller JM (2001) Appl Catal A 209:L1
45. Gomez R, Lopez T, Tzompantzi F, Garciafigueroa E, Acosta DW, Novaro O (1997) Langmuir 13:970
46. Reddy BM, Khan A (2005) Catal Rev 47:257
47. Tarafdar A, Panda AB, Pramanik P (2005) Microporous Mesoporous Mater 84:223
48. Ragauskas AJ, Williams CK, Davison BH, Britovsek G, Cairney J, Eckert CA, Frederick WJ, Hallett JP, Leak DJ, Liotta CL, Mielenz JR, Murphy R, Templer R, Tschaplinski T (2006) Science 311:484
49. Fukuoka A, Dhepe PL (2006) Angew Chem Int Ed 45:5161